Appl Magn Reson (2010) 39:357–364
DOI 10.1007/s00723-010-0166-4

Applied
Magnetic Resonance

Gamma Knife® 3-D Dose Distribution Mapping by Magnetic Resonance Imaging

Hernán J. Cervantes · Christianne C. Cavinato · Letícia L. Campos · Said R. Rabbani

Received: 23 April 2010 / Revised: 29 June 2010 / Published online: 2 October 2010

Abstract In medical processes where ionizing radiation is used, dose planning and dose delivery are the key elements to patient safety and treatment success, particularly, when the delivered dose in a single session of treatment can be an order of magnitude higher than the regular doses of radiotherapy. Therefore, the radiation dose should be well defined and precisely delivered to the target while minimizing radiation exposure to surrounding normal tissues [1]. Several methods have been proposed to obtain three-dimensional (3-D) dose distribution [2, 3]. In this paper, we propose an alternative method, which can be easily implemented in any stereotactic radiosurgery center with a magnetic resonance imaging (MRI) facility. A phantom with or without scattering centers filled with Fricke gel solution is irradiated with Gamma Knife® system at a chosen spot. The phantom can be a replica of a human organ such as head, breast or any other organ. It can even be constructed from a real 3-D MR image of an organ of a patient using a computer-aided construction and irradiated at a specific region corresponding to the tumor position determined by MRI. The spin–lattice relaxation time T_1 of different parts of the irradiated phantom is determined by localized spectroscopy. The T_1-weighted phantom images are used to correlate the image pixels intensity to the absorbed dose and consequently a 3-D dose distribution with a high resolution is obtained.

H. J. Cervantes (✉) · S. R. Rabbani
Laboratório de Ressonância Magnética, Instituto de Física, Universidade de São Paulo, Rua do Matão, Travessa E 158, Caixa Postal 66318, São Paulo, SP CEP 05315-970, Brazil
e-mail: hernan@if.usp.br

C. C. Cavinato · L. L. Campos
Gerência de Metrologia das Radiações, Instituto de Pesquisas Energéticas e Nucleares (IPEN-CNEN/SP), São Paulo, Brazil

1 Introduction

Stereotactic radiosurgery (SRS) treats brain disorders with a precise delivery of a single, high dose of radiation, causing such a powerful change in the target area that it can be considered as a "surgical" effect. To minimize the amount of radiation that passes through healthy brain tissue, the patient is highly immobilized and a three-dimensional (3-D) computer-aided planning is used. The ^{60}Co based equipments provide high accuracy in targeting and precise treatment for brain cancers. They are dedicated to treating only brain tumors and dysfunctions with a single-shot treatment. A well-known machine is the Gamma Knife®, which does not move during the treatment, thus providing a high degree of precision within the brain. It has been available for over 40 years, with constant enhancements, substantial research and follow-up backing its treatments and outcomes. The unit today is much the same as when it was developed. The machines utilize multiple sources of radiation, which causes less damage to healthy tissue and results in better targeting. To date, more than 350,000 people have received treatment with Gamma Knife® equipment, which is ideal for smaller tumors (<3.5 cm in diameter) and functional disorders of the brain.

When the cells within the live tissues are irradiated with gamma rays, the deoxyribonucleic acid, the genetic material in the nucleus of the cell, can be injured, causing alteration in the metabolism and/or the reproduction function of the cell. Therefore, when the ionizing radiation is used, either for radiotherapy or for radiosurgery, one must be sure that the healthy tissues are protected from stray radiation as much as possible [4]. In the Gamma Knife system, a narrow gamma beams with steep dose gradient are focused on some small spot, where the maximum dose is deposited, and rapid dose reduction happens in adjacent places. High geometric precision can be reached with this equipment; however, almost all tissues are irradiated to some degree and therefore a 3-D dose distribution should be calculated. In the Leksell Gamma Knife® Model-B the GammaPlan® is used, which ignores tissue inhomogeneity by assuming the human head as water equivalent [5, 6]. In this algorithm, dose distributions from the 201 gamma beams are mathematically superimposed to calculate the total level of irradiation at each point in the patient head. The dose delivered by a single beam depends on the skull shape, the linear attenuation of gamma beams in the head, dose profiles for each collimator helmet and the dose reference point in a tissue equivalent phantom [7–9]. Moreover, accurate dosimetry of small-field photon beams used in SRS can be made difficult because of the presence of lateral electronic disequilibrium and steep dose gradients. A 3-D map of the irradiated region can be measured using different strategies. In the published literature, data acquisition for radiosurgery is mainly based on diode and film dosimetry and sometimes on small ionization chamber or thermoluminescence dosimetry. These techniques generally do not provide the required precision because of their energy dependence and/or poor resolution, neither can be used to obtain a 3-D radiation dose distribution.

In this study, we present a gel dosimeter that allows one to visualize the 3-D radiation dose distribution and the corresponding isodose surfaces. In a suitable pulse sequence, the nuclear magnetic resonance (NMR) signal intensity, for the same set of experimental parameters, depends on the spin–lattice relaxation rate, which is greatly

influenced by the presence of paramagnetic ions [10]. Fricke xylenol gel (FXG) dosimetry is based on the fact that ferrous ions (Fe^{2+}) are oxidized to the ferric ions (Fe^{3+}) after being irradiated with ionizing radiation and these two ions affect NMR relaxation rate differently because they possess distinct magnetic moments, ionic radii and correlation times [11]. The concentration of ferric ions in the Fricke gel solution can be determined by magnetic resonance imaging (MRI) [12]. In the T_1-weighted MR images, the pixel intensity is directly proportional to the ferric ion concentration and, therefore, directly proportional to the radiation dose. The linear dependence of the absorbed dose versus the relaxation rate ($R_1 = 1/T_1$) and the absorbed dose versus the pixel intensity up to 50 Gy are shown in Ref. [12]. In this work, the samples were irradiated up to 100 Gy. It is shown that the pixel intensity is linearly proportional to the absorbed dose up to 80 Gy.

A single-neck round-bottom flask phantom was filled with Fricke gel solution and irradiated with a Gamma Knife system. The MRI pixel intensity and the corresponding spin–lattice relaxation time in different regions of the phantom were measured. In this way, the absorbed radiation dose was correlated to the pixel intensity and a 3-D map of absorbed dose was generated. There are several other methods for 3-D radiation dose mapping [3, 5–9], in particular, the one proposed by Gustavsson et al. [13] that uses MRI. They determine the radiation dose in each individual image pixel by determination of corresponding relaxation time, which is very time consuming. In our method, one has to determine the relaxation time only in two voxels for the intensity versus radiation dose calibration.

2 Materials and Methods

The FXG gel solution was prepared as described by Galante et al. [12], and a single-neck round-bottom flask of 1000 mL with a diameter of approximately 12.5 cm was filled with this solution up to the neck and stored under refrigeration, (4 ± 1) °C, and light protected during about 12 h after preparation. After this period, the flask was maintained 30 min at room temperature and light protected in order to reach thermal equilibrium before being irradiated. Subsequently, the flask was placed in the stereotactic frame and introduced into the Leksell Gamma Knife Model-B at the "Instituto de Radiocirugia Neurólogica" in São Paulo City. The dose planning system of the Gamma Knife Model-B, Leksell GammaPlan®, was used to calculate the delivered dose assuming skull geometry. The irradiated volume within the phantom and the radiation dose were chosen to simulate a realistic tumor treatment. A sphere of approximately 6 cm^3, located at $x = 84.0$ mm, $y = 54.0$ mm and $z = 82.0$ mm in relation to the reference point ($x = 82.0$ mm, $y = 50.0$ mm and $z = 100.0$ mm) fixed at the stereotactic frame was irradiated with ^{60}Co for 59.68 min. This dose corresponded to 40 Gy, the prescribed 50% isodose surface overlapping the sphere surface (the irradiated dose at the center of the sphere corresponded to 80 Gy). After irradiation, the flask was kept in a box containing ice and transported to the MRI facility center. Due to the distance between the irradiation center and the MRI facilities, the images were obtained 3 h after the irradiation. The MR images were obtained at the "Laboratório de Ressonância

Magnética, Instituto de Física da Universidade de São Paulo" in São Paulo City, using a Philips Gyroscan S15/ACS scanner of 1.5 T. Two series of images were acquired, one before the flask was irradiated and another 3 h after irradiation. These were used to build up the 3-D images. The former series of images was used as a reference to correct the artifact due to the head coil radio-frequency inhomogeneity. The second series was obtained with the irradiated flask placed at the same position within the magnet. The images were obtained using the spin-echo sequence with a repetition time (TR) of 700 ms and an echo time (TE) of 11 ms, slice thickness of 4 mm, field of view (FOV) of 160 mm with 256 points in each direction and 33 slices. The scan duration was 1 h 12.24 min.

3 Results

The pixel brightness was associated with the radiation dose through a calibration curve, which was obtained as follows. Using gamma rays from a ^{60}Co source, several cuvettes containing the FXG solution were irradiated with predetermined doses between 0 and 100 Gy at the Instituto de Pesquisas Energéticas e Nucleares (IPEN). These were placed in a polystyrene set up and their T_1-weighted MR images were obtained and the spin–lattice relaxation time of the content of each cuvette also was measured by localized NMR spectroscopy. In this way, the calibration curve R_1 ($1/T_1$) versus the radiation dose presented in our previous paper [12] was extended to cover the interval between 0 and 100 Gy. The T_1-weighted images of 32 cuvettes irradiated with different doses are presented in Fig. 1. Figure 2a and b shows the calibration curves of R_1 ($1/T_1$) versus the radiation dose and the pixel intensity versus the radiation dose, respectively.

The effect of the radiation in a phantom is clearly shown in Fig. 3. An MR image of a selected slice of the phantom before being irradiated is presented in Fig. 3a, while the image of the same slice after being irradiated is shown in Fig. 3b. As seen in Fig. 3b, there is a drastic change in the MRI pixel intensity corresponding to the region of the phantom where the gamma radiation was focused. A 3-D image of the FXG phantom after being irradiated is shown in Fig. 4. There will always be a fading effect due to the diffusion of the Fe^{3+} ions from the irradiated region to the non-irradiated one. The dynamics of this process depends on several factors, which eventually will be represented by the diffusion coefficient of the Fe^{3+} ions through the phantom. In our case, the diffusion coefficient was large enough to allow us to obtain the MR image of the irradiated phantom within 3 h without appreciable fading degradation [14]. Actually, we tried to improve our preparation methods to produce new Fricke gel solutions with much slower diffusion coefficient.

To obtain the isodoses curves, the spin–lattice relaxation time T_1 was measured in two voxels of $10.0 \times 10.0 \times 10.0$ mm^3: one at the center of the spot where radiation is maximum and the other at the opposite side of the sphere as shown in Fig. 3b. The obtained values were $T_1 = (323.4 \pm 2)$ ms and $T_1 = (882.8 \pm 15)$ ms, respectively. As seen in Fig. 2, these values correspond to radiation doses of (83 ± 6) and (6 ± 4) Gy, respectively. The radiation doses were related to the pixel intensities as follows:

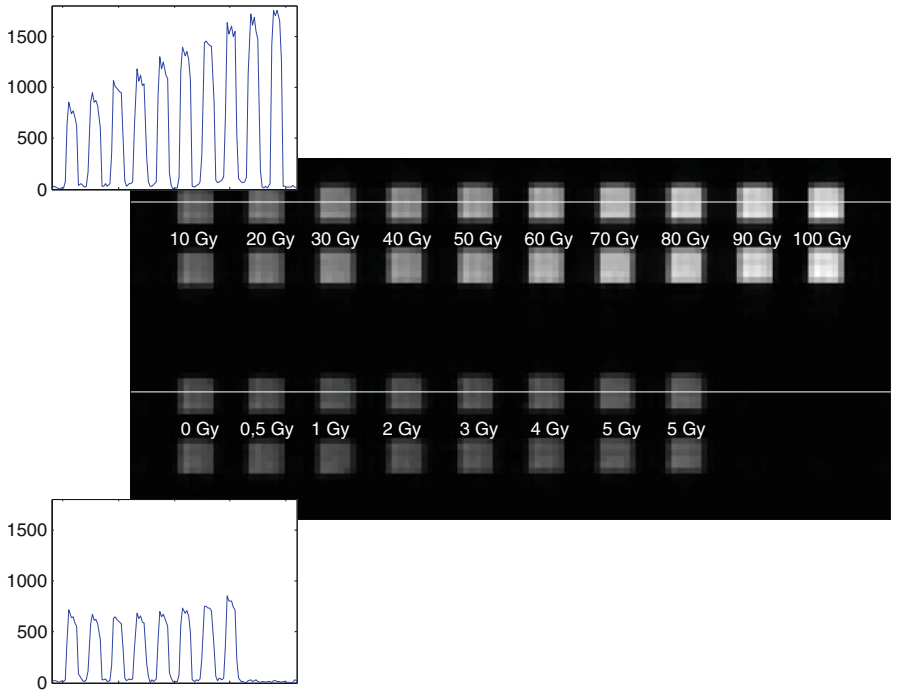

Fig. 1 Calibration image. T_1-weighting images of 32 cuvettes irradiated with different doses. The cuvettes were prepared and irradiated as described in Ref. [12]. The two superior rows of cuvettes were irradiated pairwise; therefore, there are only ten points corresponding to 10, 20, 30, 40, 50, 60, 70, 80, 90 and 100 Gy radiation doses. The last two rows of cuvettes also were irradiated pairwise with very low doses (0, 0.5, 1, 2, 3, 4, 5 Gy); the only point used from these two rows in Fig. 2 corresponds to the zero radiation point. The insets show the MRI pixel intensities of different cuvettes for each row

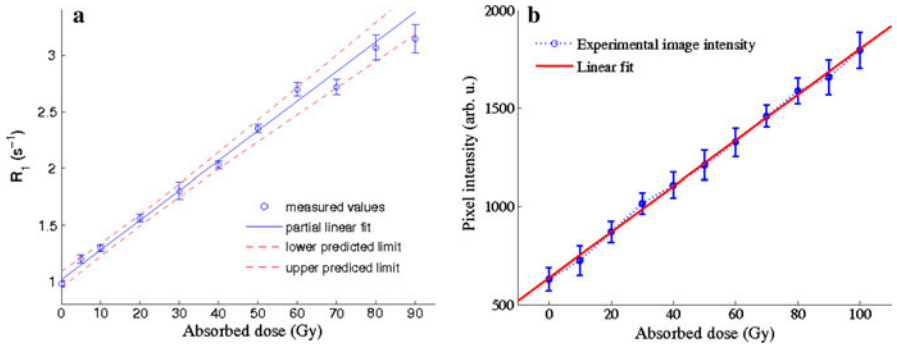

Fig. 2 **a** Relaxation rate versus the radiation dose. *Open circles* represent experimental data. A linear regression was used to generate the theoretical curve (*solid line*). **b** The Pixel intensity versus the radiation dose. *Full circles* represent the experimental data. A linear regression was used to generate the theoretical curve (*solid line*). In both plots, the lower and upper limits are shown (*dashed line*)

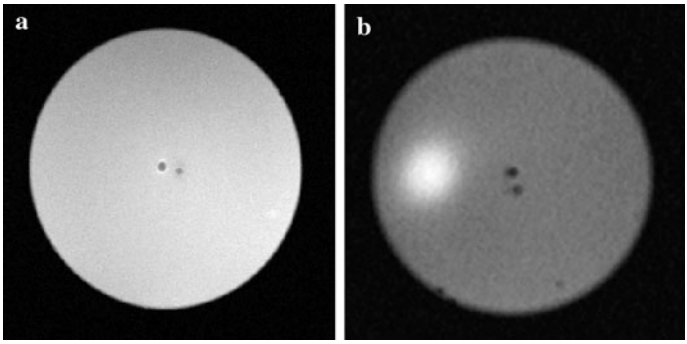

Fig. 3 MR image of a single slice of the FXG phantom before (**a**) and after (**b**) irradiation. Images were obtained by a spin-echo sequence with TR = 700 ms and TE = 11 ms

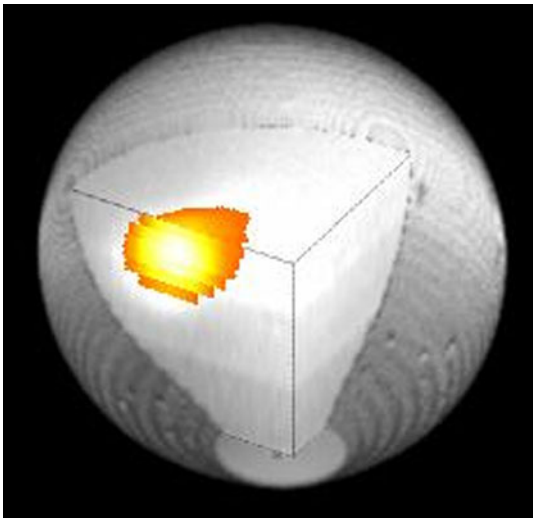

Fig. 4 3-D absorbed dose reconstruction showing the irradiated point of the simulated treatment

(a) To correct the eventual artifacts due to the equipment and/or the phantom preparation, the images of different slices after irradiation were divided by the corresponding images before irradiation, pixel by pixel;
(b) Since the measured relaxation time corresponded to an average taken over a volume of 1 cm^3, this value was compared to the average intensity of the voxels filling the same volume;
(c) Since the pixel intensity is directly proportional to the relaxation rate, it is linearly proportional to the radiation dose;
(d) Finally, the intensity of each pixel is calculated and the isodose surfaces are traced.

The isodose curve for the slice passing through the center of the sphere and the center of the irradiated volume is shown in Fig. 5, and a 3-D image of the irradiated volume is shown in Fig. 4.

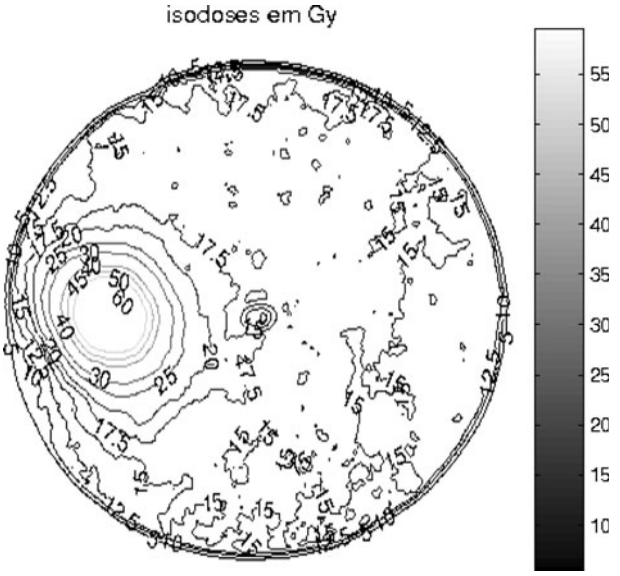

Fig. 5 Isodose curves of slice passing through the sphere center and the irradiated spot. The image intensity changes corresponding to the same slice are shown in Fig. 3b

4 Conclusion

The pixel intensity of MRI can be used to determine the isodose surfaces in an irradiated phantom and consequently a 3-D dose distribution can be obtained. The advantage of the proposed method is that it can easily be implemented in any MRI scanner and the phantoms can be as realistic as one desires. The results obtained by using a human skull filled with FXG solution and irradiated in different regions will be presented in another paper where the human head details are simulated by introducing in the skull different objects, such as nitrogen-filled blooms to simulate the cavities or pieces of bones to simulate the head's bone structures. In literature, several other methods have been proposed; however, none of these is as sensitive as this one and none presents the same spatial resolution.

Acknowledgments We thank the authors would like to thank the Instituto de Radiocirurgia Neurológica of the Santa Paula Hospital for allowing us to use their Gamma Knife facilities. This work received the support of Fundação de Amparo à Pesquisa do Estado de São Paulo and Conselho Nacional de Desenvolvimento Científico e Tecnológico.

References

1. J.J. Novotny, V. Spevacek, P. Dvorak, J. Novotny, J. Hrbacek, J. Tintera, J. Vymazal, T. Cechak, J. Michalek, J. Vacik, R. Liscak, Radiother. Oncol. **68**, S51–S81 (2003)
2. M.A. Bero, W.B. Gilboy, P.M. Glover, H.M. El-Masri, Nucl. Instrum. Methods Phys. Res. B **166**, 820–825 (2000)
3. F. Isbakan, Y. Ülgen, H. Bilge, Z. Ozen, O. Agus, B.F. Buyuksarac, Med. Phys. **34**(5), 1623–1630 (2007)

4. D. Cukier, *Chemotherapy and Radiation Therapy* (McGraw-Hill, Blacklick, 2005)
5. W.K. Kan, P.M. Wu, H.T. Leung, T.C. Lo, C.W. Chung, D.L.W. Kwong, S.T. Sham, Phys. Med. Biol. **43**(3), 529–537 (1998)
6. V. Moskvin, R. Timmerman, C. DesRosiers, M. Randall, P. DesRosiers, P. Dittmer, L.V. Papiez, Phys. Med. Biol. **49**(21), 4879–4895 (2004)
7. A. Wu, G. Lindner, A.H. Maitz, A.M. Kalend, L.D. Lunsford, J.C. Flickinger, W.D.A. Blooner, Int. J. Radiat. Oncol. Biol. Phys. **18**(4), 941–949 (1990)
8. A. Wu, Neurosurg. Clin. N. Am. **3**, 335–350 (1992)
9. M. Heydarian, P.W. Hoban, A.H.M. Beddoe, Phys. Med. Biol. **41**(1), 93–110 (1996)
10. S.R. Rabbani, Phys. Rev. B **27**(3), 1493–1497 (1983)
11. J.C. Gore, Y.S. Kang, R.J. Schulz, Phys. Med. Biol. **29**(10), 1189–1197 (1984)
12. A.M.S. Galante, H.J. Cervantes, C.C. Cavinato, L.L. Campos, S.R. Rabbani, Rad. Meas. **43**(2–6), 550–553 (2008)
13. H. Gustavsson, A. Karlsson, S.A.J. Back, L.E. Olsson, P. Haraldsson, P. Engstrom, H.H. Nystrom, Med. Phys. **30**(6), 1264–1271 (2003)
14. H.J. Cervantes, A. C. Bloise, S.R. Rabbani, Appl. Magn. Reson. **38**(4), 417–429 (2010)